



HAL
open science

Dissection of Dom34–Hbs1 reveals independent functions in two RNA quality control pathways

Antonia M G van den Elzen, Julien Henri, Nouredine Lazar, María Eugenia Gas, Dominique Durand, François Lacroute, Magali Nicaise, Herman van Tilbeurgh, Bertrand Séraphin, Marc Graille

► To cite this version:

Antonia M G van den Elzen, Julien Henri, Nouredine Lazar, María Eugenia Gas, Dominique Durand, et al.. Dissection of Dom34–Hbs1 reveals independent functions in two RNA quality control pathways. *Nature Structural and Molecular Biology*, 2010, 17, pp.1446 - 1452. 10.1038/nsmb.1963 . hal-03298535

HAL Id: hal-03298535

<https://hal.science/hal-03298535>

Submitted on 23 Jul 2021

HAL is a multi-disciplinary open access archive for the deposit and dissemination of scientific research documents, whether they are published or not. The documents may come from teaching and research institutions in France or abroad, or from public or private research centers.

L'archive ouverte pluridisciplinaire **HAL**, est destinée au dépôt et à la diffusion de documents scientifiques de niveau recherche, publiés ou non, émanant des établissements d'enseignement et de recherche français ou étrangers, des laboratoires publics ou privés.

Dissection of the Dom34-Hbs1 complex reveals independent functions in two cytoplasmic RNA quality control pathways

Antonia M.G. van den Elzen^{1,2,*}, Julien Henri^{3,*}, Nouredine Lazar³, María Eugenia Gas^{1,2}, Dominique Durand³, François Lacroute¹, Magali Nicaise³, Herman van Tilbeurgh³, Bertrand Séraphin^{1,2,#} and Marc Graille^{3,#}.

1. Equipe Labellisée La Ligue, Centre de Génétique Moléculaire (CGM). CNRS 1 avenue de la Terrasse 91198 Gif-sur-Yvette Cedex. France

2. and, IGMBC (Institut de Génétique et de Biologie Moléculaire et Cellulaire), Illkirch F-67400, France; CNRS, UMR7104, Illkirch F-67404, France; Inserm, U964, Illkirch F-67400, France; and Université de Strasbourg, Strasbourg F-67000, France

3. Institut de Biochimie et Biophysique Moléculaire et Cellulaire (IBBMC). CNRS UMR8619 Bat 430 Université Paris Sud 91405 Orsay Cedex. France

* Both authors contributed equally.

Correspondance should be addressed to : seraphin@igbmc.fr or marc.graille@u-psud.fr

Abstract.

Eukaryotic cells have evolved several quality control pathways relying on translation to detect and degrade defective RNAs. The Dom34 and Hbs1 proteins, related to translation termination factors, are involved in No-Go decay (NGD) and non-functional 18S rRNA decay (18S NRD), pathways that eliminate RNAs causing strong ribosomal stalls. We have solved the structure of Hbs1^{+/}-GDP and obtained a low-resolution model of the Dom34-Hbs1 complex. This complex mimics elongation factor-tRNA and translation termination eRF1-eRF3 complexes supporting that it binds to ribosomal A-site. We further show that nucleotide binding by Hbs1 is essential for NGD and 18S NRD. Surprisingly, Hbs1 mutants disrupting Dom34-Hbs1 interaction strongly impair NGD but have almost no effect on 18S NRD. Hence, NGD and 18S NRD can be genetically dissociated suggesting that mRNA and rRNA present in a stalled translation complex may not always be simultaneously degraded.

The transfer of genetic information from DNA into functional RNAs requires a multi-step combination of transcription and processing in eukaryotes. These processes are sources of errors that potentially affect the overall accuracy of gene expression. To minimize these defaults that *in fine* may lead to cell death or diseases, eukaryotic cells have developed several quality-control mechanisms aimed at detecting and degrading these non-functional RNAs ^{1,2}.

For example nonsense-mediated decay (NMD) targets for degradation faulty mRNAs harboring in-frame premature termination codons, that if translated could produce deleterious truncated proteins ^{2,3}. NMD functions through the interplay between the translational apparatus (ribosome, release factors eRF1 and eRF3...) and specific NMD factors (Upf1-3, Smg1, Smg5-7) which recruit the mRNA degradation machineries. Aberrant mRNAs that are devoid of in-frame stop codons are degraded by the non-stop decay pathway (NSD). NSD facilitates the recycling of the ribosomes stalled at the 3' end of these mRNAs and requires Ski factors and the exosome ^{4,5} as well as an E3-ubiquitin ligase that is implicated in the degradation of the cognate aberrant polypeptides ⁶.

More recently, two novel RNA surveillance pathways that turned out to involve identical factors have been described in yeast. First, Doma & Parker described that mRNAs containing an engineered stable stem loop that forces the ribosome to pause during elongation are rapidly degraded. Endonuclease cleavage in the vicinity of the stem loop is followed by 5'→3' degradation of the 3' cleavage product by the exonuclease Xrn1 and 3'→5' degradation of the 5' cleavage product dependent on Ski7 and the Ski complex that in turn recruit the exosome ⁷. This pathway, named No-Go Decay or NGD, also targets depurinated mRNAs, a chemical damage that also induces ribosome stalling ⁸. NGD involves at least the proteins Dom34 and Hbs1 ⁷ that are related to translation termination factors eRF1 and eRF3 respectively.

In parallel, Dom34 and Hbs1 have been implicated in the 18S NRD pathway ^{9,10}. This surveillance mechanism degrades non-functional 18S rRNAs that are able to associate into ribosomal subunits but incapable of supporting efficient translation. This pathway also targets ribosomes containing immature 20S pre-rRNAs that engage in translation ¹¹. Neither Dom34 nor Hbs1 are required for efficient growth in the yeast *Saccharomyces cerevisiae*. However, deletion of *HBS1* or *DOM34* have been demonstrated to cause severe growth defects in strains containing a null allele for one out of several genes encoding proteins of the small ribosomal subunit (*RPS30A*, *RPS30B*, *RPS14A*) ¹². These strains are still viable as pairs of genes encode the corresponding ribosomal proteins. However, in deleted strains the remaining gene copy is probably insufficient to maintain a proper balance of the corresponding ribosomal protein. This would lead to the accumulation of incomplete/unstable small ribosomal subunit predisposed to stalling. Hence, growing evidence points towards a role of Dom34 and Hbs1 proteins in clearing cells from RNAs inducing translational stalls, i.e. poorly functional small ribosomal subunits, mRNAs with in-frame stable stem loops and depurinated RNAs.

Studies in yeast, fruit fly and mouse have shown that Dom34 (also known as Pelota in higher eukaryotes) is required for correct mitotic and meiotic cell division¹³⁻¹⁶. Dom34/Pelota is structurally related to the translation termination factor eRF1 with the exception of its N-terminal domain that adopts a Sm-fold, commonly found in proteins involved in RNA recognition or degradation^{17,18}. This domain was proposed to exhibit an *in vitro* divalent metal ions endonuclease activity¹⁸ but this finding was recently challenged¹⁹. First, the *in vitro* nuclease activity previously observed for the yeast Dom34 protein could not be reproduced. Second, over-expression of the Rps30a protein was sufficient to restore some mRNA cleavage in the absence of Dom34.

Dom34 associates with Hbs1, a member of the family of eEF-1A-like GTPases including translation elongation factors eEF-1A and EF-Tu that deliver amino acyl-tRNAs to the ribosomal A-site, eRF3, and Ski7^{12,17,20,21}. Initially, Hbs1 was identified as Hsp70 subfamily B suppressor. In yeast, deletion of both *SSB1* and *SSB2* genes (encoding Hsp70 chaperones interacting with the nascent polypeptide chain at the exit of the ribosome channel during protein synthesis) results in slower cell growth, in the decrease of the number of translating ribosomes and in slower translation²². This phenotype is suppressed by over-expression of Hbs1 suggesting that Hbs1 may help in stop codon-independent peptide release from ribosomes stalled by the absence of Hsp70-mediated nascent polypeptide channeling, a function closely related to the one proposed for Hbs1 and Dom34 in both NGD and 18S NRD²³. Hbs1 is a GTP binding protein whose affinity for GTP but not GDP is enhanced by Dom34, similarly to the effect of eRF1 on eRF3 binding to GTP^{12,17,24}.

To gain insight into the mechanism of the Dom34-Hbs1 complex in these quality control pathways, we have solved the crystal structure of yeast Hbs1 and obtained a low-resolution model of the Dom34-Hbs1 complex by SAXS. This allowed a precise study of the role of Hbs1 nucleotide binding site and interaction with Dom34 in NGD and 18S NRD, which demonstrated, interestingly, that these two processes could be genetically separated.

Results

Overall structure

As the N-terminal region of *S. cerevisiae* Hbs1 is predicted to be poorly folded, we have purified several Hbs1 fragments starting at different positions. Diffracting crystals could only be obtained for a fragment encompassing residues 135-610 (hereafter named Hbs1dN134). Its structure was solved using the SAD method (see Supplementary Fig. 1 for experimental electron density maps). The structures of the apo and GDP bound forms were further refined to 2.5Å and 2.95Å resolution, respectively (Supplementary Table 1). As expected from sequence analysis, Hbs1 is a member of the eEF-1A protein family. Hbs1dN134 is composed of a N-terminal GTPase domain (residues 165 to 375) and two 6-stranded β -barrel domains (domain II from residue 399 to 498 and domain III from residue 499 to 610; Fig. 1a). The GTPase domain is preceded by a long N-terminal loop (residues 140 to 164) partially folded as an α -helix (α A), which packs against domain II. The GTPase domain adopts the classical α/β structure common to GTPases such as EF-Tu, eRF3 and Ras^{25,26}. It is composed of a central six-stranded β -sheet (strands order β 6, β 5, β 4, β 1, β 3 and β 2, which is antiparallel to the others) flanked by 7 α -helices (α 1, α 2, α 6 and α 7 on one side of the sheet and α 3 to α 5 on the other). It is connected to domain II by a long α helix (α 7; residues 376 to 398). Both domains II and III adopt a fold similar to the corresponding domains from EF-Tu and eRF3^{25,27}. In all structures of bacterial and eukaryotic members from the eEF-1A superfamily, domains II and III are held together in the same relative orientation but this is not true for the GTPase domain. In the structure of *S. pombe* eRF3, there are no contacts between the GTPase domain and domains II and III²⁵ (Supplementary Fig. 2a). In the case of Hbs1dN134, the GTPase domain packs against the domains II and III in a manner highly reminiscent of the EF-Tu-GDPNP complex. Small-angle X-ray scattering experiments (SAXS) in solution on Hbs1dN134 show that the Hbs1 conformation observed in our crystal structure fully agrees with the conformation of the protein in solution and hence is not induced by crystal packing (see supplementary data, Supplementary Fig. 2)

The nucleotide binding site

Similarly to the other members of the eEF-1A family, Hbs1 is a GTP binding protein^{12,17}. We have solved the structure of Hbs1dN134 either in its apo-form or in the presence of GDP. As observed for archaeal SelB elongation factor and eukaryotic release factor eRF3^{25,28}, no large-scale domain movements are observed between the apo and GDP bound forms of Hbs1dN134 (rmsd of 0.4 Å over 430 C α atoms).

GTPases are characterized by the presence of a P-loop and two highly flexible and conserved segments called switch regions I and II that are directly involved in nucleotide binding. They adopt radically different conformations depending on which nucleotide is bound (GDP or GTP). The structure of the switch regions of GTPases is highly variable for the GDP forms but invariant for the

GTP forms²⁶. In the Hbs1dN134 apo-form, switch I (residues 194-234) is mostly disordered (absence of electron density for the region 205-228) although its N-terminal part folds as a helix ($\alpha 2$). Upon GDP binding, a portion from this switch (residues 217-228) folds as a small α -helix ($\alpha 2'$, residues 217-223) antiparallel to helix $\alpha 2$ (Fig. 1b). Switch II (residues 251-268) forms an α -helix ($\alpha 3$) connected to strand $\beta 3$ by a loop. The orientation of helix $\alpha 3$ remains constant between the apo and GDP bound forms but the $\beta 3$ - $\alpha 3$ loop (residues 251-258) exhibits some flexibility (Fig. 1b, Supplementary Fig. 3). Most of Hbs1 residues contacting GDP structurally match with the corresponding residues in the *E. coli* EF-Tu – GDP complex²⁹ (Fig. 1c). The P-loop coordinates the GDP phosphate groups via the main chain atoms from residues Val176 to Thr182 and side chains from polar residues (Asp177, Ser181 and Thr182). The guanine base is stacked between the hydrophobic moieties from Lys314 and Phe354. In the EF-Tu GDP complex, switch II contacts the Mg^{2+} ion. This is not the case for the Hbs1dN134 GDP complex as Mg^{2+} has been omitted in our experiments due its inhibitory effect on GDP binding to Hbs1 (data not shown).

Two point mutants of the nucleotide binding site (V176G from the P-loop and H255E of the switch II region) were previously shown not to complement a *HBS1* deletion, suggesting that nucleotide binding is required for Hbs1 function¹². As stated above, Val176 is part of the P-loop and is involved in phosphate binding. In the Hbs1dN134-GDP complex, His255 is not directly in contact with GDP but it may play a crucial role for GTP binding and/or hydrolysis. To characterize the effect of these mutations on nucleotide binding, we have produced three single point mutants (V176G, H255E as well as K180A from the P-loop). We then tested their ability to bind guanine nucleotides by isothermal titration calorimetry (ITC). No significant nucleotide binding to the mutants could be observed compared to the wild-type protein (Supplementary Fig. 4a-b). Circular dichroism (data not shown) and differential scanning calorimetry measurements (DSC) on these mutants suggest they are correctly folded (Supplementary Table 6 and Supplementary Fig. 4c). We conclude that the substitutions introduced completely abolish nucleotide binding.

Low-resolution model of the Dom34-Hbs1 complex.

Hbs1 and Dom34, as is the case for eRF3 and eRF1, physically interact together^{12,17}. The recent crystal structure of the complex between eRF1 and an eRF3 fragment lacking the GTPase domain confirmed that the eRF1-eRF3 interface is located between the eRF1 C-terminal domain and the eRF3 domain III³⁰. We suggest that the formation of the Hbs1-Dom34 complex very likely occurs via the corresponding domains. Superimposition of these Dom34 and Hbs1 domains onto the structure of the eRF1-eRF3 complex strongly argues in favor of the involvement in complex formation of residues from loops connecting strands $\beta A'$ to $\beta B'$ and $\beta C'$ to $\beta D'$ from Hbs1 (Fig. 1d). In this model, these loops face residues from the C-terminal part of helix $\alpha 7$, from $\alpha 11$ as well as strand $\beta 13$ from Dom34.

To validate our Dom34-Hbs1 interaction model, we have assessed the effect of introducing domain deletions in Dom34 (C-terminally Strep-tagged) on the interaction with Hbs1 (C-terminally His₆-tag) after co-expression in *E. coli*. Strep-Tactin sepharose affinity purification demonstrates that Hbs1 is retained on the column only when co-expressed with Dom34 (Supplementary Fig. 5a-b). Deletion of the N-terminal or central domain does not strongly affect complex formation (Supplementary Fig. 5c-d). In contrast, deletion of Dom34 C-terminal domain almost completely abolished complex formation, indicating that this domain is crucial for the interaction with Hbs1, similar to the role of eRF1 C-terminal domain in eRF3 binding (Supplementary Fig. 5e; ³⁰).

In order to get further insight into how Hbs1 and Dom34 might interact, we have performed SAXS measurements on the Dom34-Hbs1dN134 complex (Fig. 2a and Supplementary Fig. 6a). From the crystal structures of yeast and archaeal Dom34 (comparison of these structures revealed large conformational changes), yeast Hbs1dN134 and of the eRF1-eRF3 complex ^{17,18,30}, we have generated two initial models (yeast-like and archaeal-like) for the Dom34-Hbs1dN134 complex and compared the corresponding experimental and calculated scattering curves (see supplementary files for details on the different models and Supplementary Fig. 6b-c for a representation of the initial models). The best agreement with the experimental scattering curve is obtained for the archaeal-like model (Fig. 2a; χ value of 5.9 vs 13.4 for the yeast-like model). In addition to the contacts between the Dom34 C-terminal domain and the Hbs1 domain III, this model highlights contacts between the Dom34 central domain and the Hbs1 GTPase domain in this model. We have performed rigid-body modelling with the program SASREF ³¹ to improve the fit between calculated and experimental curves (Fig. 2a-b, χ values ≤ 1.7 , see supplementary files for details). The resulting models show that in the Dom34-Hbs1 complex, Dom34 adopts a tRNA-shape with its N-terminal and central domains matching with the anticodon and amino acyl acceptor arms of a tRNA molecule, respectively, as observed in the EF-Tu – tRNA complex (Fig. 2b-c; ²⁷). This further suggests that Dom34-Hbs1 binds into the ribosomal A site.

Nucleotide binding by Hbs1 is crucial for 18S NRD and NGD.

Several studies on members of the eEF-1A family have already demonstrated the critical role of GDP/GTP binding for their function. Consistently, two point mutations within Hbs1 GDP binding site (V176G and H255E), which abolish nucleotide binding (Supplementary Fig. 4), do not complement a *HBS1* deletion ¹². To investigate further the importance of nucleotide binding by Hbs1 in NGD and 18S NRD, we have tested the physiological importance of Hbs1 mutations affecting nucleotide binding (V176G and H255E and K180A) by examining the effect of these point mutants on NGD, 18S NRD and growth in strains deleted for small ribosomal subunit genes in *S. cerevisiae*.

We first constructed a protein A tagged version of Hbs1 that allowed us to assess expression of wild-type and mutant proteins. The wild-type Hbs1-ProtA fusion was shown to be indistinguishable from wild type in all assays (see below). Mutants V176G, K180A and H255E were produced normally in

yeast cells (Supplementary Fig. 7a) while DSC measurements are characteristic of well folded proteins with a peak centered at a T_m of 47°C, i.e. 8.8°C lower than wild type Hbs1 protein (Supplementary Table 6 and Supplementary Fig. 4c). To examine the effect of these mutants on NGD, we used an assay described before¹⁹. The degradation of a NGD substrate starts with an endonucleolytic cleavage in the vicinity of the stalled ribosome. In a *ski7Δ* strain, the 5' endonucleolytic cleavage product of NGD substrate PGK1-SL (PGK1 containing a stem-loop) accumulates in a manner dependent upon the presence of both Dom34 and Hbs1^{7,19}. We assayed whether Hbs1 mutants abolishing nucleotide binding could restore accumulation of this degradation intermediate in a *ski7Δhbs1Δ* strain. In presence of our mutants, the ratio of degradation intermediate to full-length reporter mRNA was reduced to 30% of the ratio observed in presence of wild type Hbs1, a level similar to the one detected in absence of Hbs1 (Fig. 3a lanes 4-6 and c).

The rapid degradation of the 18S NRD substrate 18S A1492C has been shown to depend at least partly on the presence of both Dom34 and Hbs1¹⁰. In absence of one or the other of these factors, 18S A1492C RNA steady state levels were increased (Fig. 4a-b, compare lanes 1 to lanes 2 and 3). We tested whether the Hbs1 mutants unable to bind nucleotide could restore 18S A1492C degradation in an *hbs1Δ* strain and found that they could not (Fig. 4a lane 4-6 and c), leading to steady state levels 3 to 4 fold higher than in presence of wild type Hbs1 (Fig. 4a lane 2,3) and similar to the level observed in absence of Hbs1 (Fig. 4a lane 1).

Screening for mutations generating a synthetic growth phenotype in a *dom34Δ* background identified mutations in genes encoding the Rps28 proteins of the small ribosomal subunit (data not shown). This finding is consistent with previous observations of a severe growth defect observed when deletion of *DOM34* or *HBS1* were combined with deletion of one out of several 40S subunit protein encoding genes¹². In accordance with these earlier data, the V176G and H255E mutants could not complement the slow growth of an *rps28Δhbs1Δ* strain (Fig. 4e, compare with strain expressing wild-type Hbs1). The K180A mutant proved also to be non-functional in this assay (Fig. 4e).

In conclusion, Hbs1 mutants that abolish nucleotide binding are functionally inactive in the three assays that we used. We conclude that Hbs1 nucleotide binding is essential for NGD endonucleolytic cleavage, 18S rRNAs NRD and for the function of Hbs1 required in strains lacking a gene encoding a ribosomal protein of the small subunit.

Role of the Dom34-Hbs1 interaction in NGD and 18S NRD.

Our SAXS and deletion analysis are consistent with the idea that the Dom34 and Hbs1 interaction is mediated mainly through the C-terminal domain of Dom34 and domain III of Hbs1, in a way similar to the eRF1- eRF3 interaction. To test the functional importance of the Dom34-Hbs1 interaction, we designed several mutants targeting residues of the proposed interaction surface (Y300A/E361A, E361R and E361R/Q364A in Dom34 and R517E, L520R and R557A/H558A in Hbs1, Fig. 1d) and tested their effects on NGD, NRD and growth in an *rps28Δ* strain in the assays described above.

According to our Dom34-Hbs1 interaction model that fits best with results of SAXS measurements on the Dom34-Hbs1dN134 complex, the Dom34 central domain also contacts the GTPase domain from Hbs1. To address the functional importance of this interaction we also mutated this hypothetical interaction surface. In the Dom34 central domain, a conserved loop rich in basic residues (¹⁷⁴KKKR¹⁷⁷) was mutated into alanines (KKKR mutant). While this work was in progress, the same mutation was independently shown to strongly reduce NGD¹⁹. Mutations of similarly positioned basic residues in eRF1 affect eRF3 GTPase activity, eRF1-eRF3 interaction and function³⁰. In our model this loop could contact the γ -phosphate of a GTP molecule bound to Hbs1. We also mutated a highly conserved ²¹²SPGF²¹⁵ motif in the central domain of Dom34 into AAGA (SPGF mutant). Mutation of the PGF peptide or of the proline alone was independently shown to reduce NGD¹⁹. In our structural model the SPGF motif could face a conserved ²⁵⁶RDF²⁵⁸ motif from Hbs1 GTPase domain, which we also mutated into alanines (RDF mutant, Supplementary Fig. 8). Using a yeast two-hybrid approach we confirmed that these mutants have greatly reduced interaction with their wild type partner (Supplementary Fig. 7b).

To verify whether mutants are expressed in *S. cerevisiae*, Dom34 mutants were introduced in a construct carrying a C-terminal 3HA-tag while, as described above, Hbs1 mutants contained a C-terminal protein A-tag. For each mutant, protein expression in yeast was assayed by western blotting and proteins stability measured by DSC analysis. All Hbs1 mutants as well as E361R and to a lesser extent KKKR and SPGF Dom34 mutants were expressed in yeast (Supplementary Fig. 7a) whereas lower amounts of Y300A/E361A and E361R/Q364A Dom34 mutants were detected. DSC experiments confirmed that all Hbs1 mutants behave similarly as wild-type protein (Supplementary Table 6 and Supplementary Fig. 4c). For Dom34, we could not obtain sufficient quantities of recombinant SPGF mutant to analyze its stability by DSC. All other Dom34 constructs were very similar, the Y300A/E361A, E361A/Q364R and E361R mutants being only slightly less stable than the KKKR mutant and wild type proteins (Supplementary Table 6 and Supplementary Fig. 4d).

All mutants of the interaction surfaces caused a reduction in NGD (Fig. 3a lanes 7-10, b-d). The ratio of degradation intermediate to full-length reporter mRNA was decreased to the same extent as observed in strains lacking Hbs1 or Dom34 (Fig. 3a, b lane 1). Surprisingly, none of the Hbs1 mutants affected 18S NRD as the level of 18S A1492C was identical to the one observed in the presence of wild type Hbs1, i.e. 3-4 fold lower than in a strain lacking Hbs1 (Fig. 4a lanes 7-10, c). In contrast, all Dom34 mutants caused some stabilization of the 18S A1492C NRD substrate (Fig. 4b,d), even though not to the same extent as in absence of Dom34. Although we cannot exclude that stabilization of 18S A1492C NRD substrate in Dom34 Y300A/E361A and E361R/Q364A mutants results from decreased protein levels in cells, the effect of the E361R mutant, which is detectable to similar levels as wild type Dom34, suggests that Dom34-Hbs1 interaction is required for optimal 18S NRD. Interestingly, all mutants affecting interaction complemented the slow growth defect observed in *dom34* Δ *rps28A* Δ

and *hbs1Δrps28AΔ* strains, respectively (Fig. 4e), although the Hbs1 L520R mutant and all Dom34 mutants except E361R do not restore growth to the same extent as their wild type counterpart. These results indicate that the interaction between Dom34 and Hbs1 is critical for efficient NGD but is less essential for 18S NRD and growth in the context of a strain lacking a gene encoding a ribosomal protein of the small subunit.

Discussion.

Eukaryotic cells have developed several highly sophisticated surveillance pathways dedicated to the detection of non-functional or damaged molecules (DNA, RNA but also proteins), thereby leading to their repair or rapid degradation. These mechanisms and their dysfunction play crucial roles in cellular functions and disease. In this study, we focused our attention on Hbs1 and Dom34, two interacting proteins implicated in two RNA quality control pathways: NGD and 18S NRD^{7,8,10,11}. These surveillance mechanisms have in common to specifically detect and degrade RNA molecules (mRNAs or rRNAs) that cannot correctly undergo translation elongation by eukaryotic ribosomes. However, the precise mechanisms of these pathways are largely unclear.

The structure of Hbs1dN134 reported here displays the same domain organization as other members of eEF-1A family members such as eRF3, eEF-1A, Ski7 and bacterial EF-Tu. In the structure of Hbs1 and EF-Tu, the GTPase domain is tightly packed onto domains II and III (Fig. 1a) but for eRF3 the structure is “open” as the GTPase domain makes only a few contacts with domains II and III²⁵. Our SAXS data (Supplementary Fig. 2) for Hbs1 as well as mutant analysis of *S. pombe* eRF3²⁵ support, however, the existence of a conserved “closed” conformation corresponding to our crystal structure that is likely to be necessary for correct function of members of the eEF-1A family.

Like other eEF-1A factors, Hbs1 binds GTP and GDP through its GTPase domain. Hbs1 is thus likely to cycle between GTP bound, GDP bound and free forms. We observe that nucleotide binding is essential for all the Hbs1 functions that we tested namely: NGD, 18S NRD and growth complementation. In eRF3, GTP binding (stimulated by eRF1) promotes a rearrangement of the termination complex before peptide release^{24,32-34}. This leads to GTP hydrolysis followed by rapid hydrolysis of peptidyl-tRNA, peptide release, tRNA liberation and subunit dissociation^{33,35,36}. Similarly, GTP association with Hbs1 (stimulated by Dom34¹⁷) is likely to promote rearrangement of the ribosome. Our mutants of Hbs1 impairing nucleotide binding, thereby also preventing GTP hydrolysis, are likely to impede remodeling of the stalled ribosome and/or stabilize Dom34 present in the A-site. The phenotype observed for Hbs1 mutant unable to bind nucleotides suggest that such rearrangements are a prerequisite to initiate the degradation of the small ribosomal subunit or bound mRNA.

Based on the available crystal structures of eRF1-eRF3 complex, Hbs1 and Dom34 (from yeast and archaea that display radically different orientation of the central domain relative to the N and C-terminal domains), we have build two Hbs1dN134-Dom34 models by superimposing the Hbs1 and Dom34 C-terminal domains onto the corresponding regions of the eRF1-eRF3 complex (Supplementary Fig. 6b-c). SAXS experiments (Fig. 2a) show that the model where yeast Dom34 adopts the conformation observed in the archaeal Dom34 structure¹⁸, rather than the cognate structure¹⁷, is the most likely to represent the complex in solution. Interestingly, Hbs1 homologues are absent from archaea²⁰ supporting the idea that in eukaryotes Hbs1 might push Dom34 into an active

conformation. Our Dom34-Hbs1 model is not only reminiscent of the eRF1-eRF3 complex but also displays strong analogy to the bacterial EF-Tu – tRNA complex, involved in the translation elongation step ²⁷. Comparison of our Hbs1-Dom34 model and the EF-Tu-tRNA complex (Fig. 2b-c) shows that Dom34 and the tRNA have similar shape and localization relative to the GTPase domain of their respective partners. The N-ter, central and C-ter domains from Dom34 occupy similar positions as the anticodon stem, the amino acyl acceptor arm and the T stem from the tRNA, respectively. Thus, the N-terminal domain of Dom34 is likely to bind close to the mRNA codon in the A-site of stalled ribosome. This domain is structurally unrelated to the eRF1 N-ter domain and adopts an Sm-fold ^{37,38}. Two loops (residues 49-53 and 87-92) from this Dom34 domain that are functionally important for NGD pathway in yeast ¹⁹ occupy approximately the same position as the tRNA anticodon loop in our model and hence could directly contact the mRNA codon, probably in a sequence independent manner.

Our model suggests that the interaction between Hbs1 and Dom34 occurs through two surfaces: binding of Hbs1 domain III with Dom34 C-terminal domain and contacts between the Hbs1 GTPase and the Dom34 central domains. Our binding data indicate that the former is essential for interaction while the second probably plays a regulatory role. Consistently, in human, binding of the central domain of eRF1 to eRF3 stimulates GTP binding and GTPase activity of the latter ³². It has been proposed that this involves stabilization of the eRF3 switch region by eRF1 Arg192 ³⁰, therefore explaining the increase in the affinity of eRF3 for GTP in the presence of eRF1 ^{24,34}. GTP association with Hbs1 is similarly stimulated by Dom34 ¹⁷.

Interestingly, our results indicate that the interaction between Dom34 and Hbs1 is essential for NGD, but less crucial for 18S NRD or growth in a *rps28aΔ* strain. This suggests that for NGD a function of Hbs1 is required that is not essential for 18S NRD to occur. Moreover, the interaction surface present in Dom34 appears more critical for 18S NRD than the one of Hbs1. As the presence of Dom34 and Hbs1 is essential for both NGD and 18S NRD, a possible explanation for our results is that an additional factor stabilizes the Dom34-Hbs1 interaction during 18S NRD but not during NGD. Alternatively, NGD may require a tighter interaction between Dom34 and Hbs1 than 18S NRD, and thus be more affected by a weakly interacting Hbs1. It is also possible that Dom34 interacts with another factor specifically required for NGD through the interaction surface used by Hbs1, explaining the asymmetry of our mutant phenotypes.

While the corresponding mechanistic details remain to be elucidated, our data indicate importantly that NGD and 18S NRD can be genetically dissociated. Given that NGD and NRD share several factors (Hbs1, Dom34 and components of the degradation machinery) and target substrates with similar characteristics it has been proposed before that these processes occur in parallel as a consequence of inappropriate stalling of a ribosome ¹⁰. In contrast to this hypothesis our results suggest that mRNA and rRNA present in a stalled translation complex may not always be simultaneously degraded. Interestingly, the observation that growth phenotype assayed in the absence of Rps28a correlates well

with their effects on 18S NRD, but not on NGD, allows us to conclude that in these cells 18S NRD has become critical. It can be proposed that the absence of 18S NRD may be quantitatively more detrimental to cells than defective NGD: in the first case, a small fraction of stalled ribosomes may quickly have a general impact on translation by sequestering functional ribosome in dead polysomes, while in the second case, only a few mRNA and ribosomes would be affected.

Overall, our data show that eukaryotic cells use the Hbs1-Dom34 complex as mimicry of tRNA-elongation factor complex to perform RNA quality control mechanisms. Entry of the Dom34-Hbs1 complex to the A-site of the stalled ribosomes contributes to NGD and 18S NRD but the rules governing its specific recruitment are still unknown. However, our data indicate that these two processes may be functionally separated. The mechanisms controlling the outcome of Dom34-Hbs1 binding to stalled ribosome, i.e., degradation of the substrate mRNA and/or destruction of the small ribosomal subunit remain to be deciphered. Another point to be clarified relates to the issue of the incomplete proteins produced by these stalled ribosomes. During translation termination, the eRF1 central domain contributes to protein release through a universally conserved GGQ motif³⁹. As this GGQ motif is not present in Dom34, it still remains to be determined whether hydrolysis of peptidyl-tRNA and release/degradation of truncated peptides occur in NGD and/or 18S NRD.

Acknowledgments

We are indebted to K. Blondeau, B. Faivre, J. Cicolari, D. Lebert, Y. Billier, B. Bonneau and D. Rentz for technical assistance. We thank M. Moore and R. Parker for plasmid gifts and P. Vachette for helpful discussion. This work was supported by the Agence Nationale pour la Recherche (grants ANR-06-BLAN-0075-02 and ANR-07-BLAN-0093), the Association Française contre les Myopathies (AFM), La Ligue contre le Cancer Equipe Labellisée 2008, the CNRS, the ESF EUROCORES RNA Quality and the EU “3D-Repertoire” program (LSHG-CT-2005-512028). J. Henri and A.M.G. van den Elzen hold pre-doctoral grants from the Université Paris-Sud 11 and Université de Strasbourg, respectively. M.E. Gas is supported by the Spanish Ministry of Research. We acknowledge SOLEIL for provision of synchrotron radiation facilities and we would like to thank Andrew Thompson and Javier Perez for assistance with beamlines Proxima-1 and SWING, respectively.

Author contributions.

J.H., A.M.G.vdE., M.G., B.S. designed experiments. J.H., A.M.G.vdE., N.L., D.D., F.L., M.N. and M.E.G. performed experiments. J.H., A.M.G.vdE., D.D., HvT., M.G. and B.S. analyzed data and wrote the paper.

Legends to figures.

Figure 1. Hbs1 structure representation. **(a)** Ribbon representation of the Hbs1dN134 structure. For the GTPase, II and III domains from Hbs1, the rmsd values with the corresponding domains from EF-Tu and eRF3 are $\approx 2.8\text{-}3 \text{ \AA}$ over 175-190 C α atoms (25-38% sequence identity), $\approx 1\text{-}1.3\text{ \AA}$ over 80-90 C α atoms (20-30% sequence identity) and $\approx 1.4\text{-}1.7\text{ \AA}$ over 100-110 C α atoms (18-27% sequence identity), respectively. **(b)** Conformational changes of switch regions upon GDP binding. For both apo and GDP bound form of Hbs1dN134, the crystal asymmetric unit contains two molecules organized as a non-crystallographic dimer, yielding to 4 independent sets of coordinates. These 4 copies are virtually identical (rmsd $\approx 0.4\text{-}0.5\text{ \AA}$) except for the switch regions that adopt different conformations. For clarity, only the secondary structure elements for Hbs1dN134 bound to GDP are shown (beige). The P-loop and switches I and II in the Hbs1-GDP complex are colored in yellow, red and green, respectively. The conformation of these regions in the Hbs1dN134 apo forms I and II are in blue and pink, respectively. GDP is shown as balls and sticks. **(c)** Comparison of the GDP binding mode as observed in Hbs1dN134 (same color code as panel B) and EF-Tu (grey). The GDP bound to EF-Tu is shown as black sticks. **(d)** Superimposition of Dom34 C-terminal domain (green) and Hbs1 domain III (orange) from yeast proteins onto the corresponding domain from human eRF1 and eRF3 as observed in the eRF1-eRF3 complex (grey). Mutated residues are shown as sticks.

Figure 2. SAXS analysis of the Dom34-Hbs1dN134 complex. **(a)** Comparison of the scattering curves calculated from the coordinates of the yeast-like (blue), archaeal-like (green), and SASREF Dom34-Hbs1dN134 models (red) with the experimental SAXS curve (black). **(b)** Ribbon representation of the optimized Dom34-Hbs1dN134 model. Dom34 N-terminal, central and C-terminal domains are coloured in light green, green and dark green, respectively. Hbs1 GTPase, II and III domains are coloured in light blue, cyan and dark blue, respectively. Loops A, B and C from Dom34 that have been shown to be functionally important in NGD¹⁹, are indicated in yellow, orange and red, respectively. **(c)** Ribbon representation of the bacterial EF-Tu-tRNA complex²⁷. For clarity, EF-Tu and Hbs1 are shown with the same orientation. EF-Tu GTPase, II and III domains are coloured in pink, magenta and purple, respectively.

Figure 3. Effects of Hbs1 and Dom34 mutants on NGD. **(a)** Northern analysis of the steady state levels of NGD substrate PGK1-SL degradation intermediates in a *ski7 Δ hbs1 Δ* *S. cerevisiae* strain transformed with Hbs1 mutants. The PGK1-SL reporter was expressed from the plasmid pRP1251 and detected with the oligonucleotide oRP132⁷. **(b)** Northern analysis of the steady state levels of PGK1-SL reporter degradation intermediates in a *ski7 Δ dom34 Δ* *S. cerevisiae* strain transformed with Dom34 mutants. **(c)** and **(d)** Quantification of panels a and b respectively. For each mutant the ratio of 5'

intermediate over full length PGK1-SL reporter was calculated and then standardized for the ratios calculated for Hbs1-proteinA or Dom34-3HA. Average \pm SD of 3 biological replicas are shown.

Figure 4. Effects of Hbs1 and Dom34 mutants on 18S NRD and growth in ribosomal protein deletion context. **(a)** Northern analysis of the steady state levels of 18S A1492C NRD substrate in a *hbs1* Δ *S. cerevisiae* strain transformed with Hbs1 mutants. ScR1 RNAs are presented as loading controls. The 18S A1492C reporter was expressed from the plasmid pWL160-A1492C and detected by the oligonucleotide FL125⁹. **(b)** Analysis of the steady state levels of 18S A1492C NRD substrate in a *dom34* Δ *S. cerevisiae* strain transformed with Dom34 mutants. ScR1 RNAs are presented as loading controls. **(c)** and **(d)** Quantification of a and b respectively. For each mutant the ratio of 18S A1492C over scR1 signal was calculated and then standardized for the ratios calculated for Hbs1-proteinA or Dom34-3HA. Average \pm SD of 3 biological replicas are shown. **(e)** Strains deleted for both small ribosomal subunit protein Rps28A and Hbs1 (*rps28A* Δ *hbs1* Δ , left panel) or Dom34 (*rps28A* Δ *dom34* Δ , right panel) transformed with Hbs1 mutants or Dom34 mutants were spotted in 6 10-fold dilutions on YPDA plates and grown at 16°C (8 days).

Materials and methods.

Cloning, Expression, and Purification of Hbs1 proteins

The truncated version of the HBS1 gene (*YKR0084c*) deleted for the first 134 residues was amplified by PCR from *S. cerevisiae* S288C genomic DNA. An additional His₆ tag was introduced downstream of the 3' coding sequence. The PCR products were cloned into a modified pET28 vector between EagI and NotI restriction sites. The protein was expressed and purified as previously described for the full-length protein¹⁷. A seleno-methionine (Se-Met) derivative of Hbs1dN134 was expressed in Se-Met-supplemented minimal medium using the same expression system as for the native protein. The Se-Met protein was purified with the same method as for the native protein.

The full-length mutated versions (V176G, H255E, K180A) of the HBS1 gene (*YKR0084c*) were amplified by PCR from *S. cerevisiae* expression plasmids and inserted in an ampicillin resistant pET21a vector. An additional His₆ tag was introduced downstream of the 3' coding sequence between BamHI and NotI restriction sites. The mutants were expressed and purified using the same protocol as the Hbs1dN134 protein. See further details in Supplementary Material and Methods.

Yeast strains and plasmids

All yeast strains were constructed by standard methods and are derivative of BMA64 (Supplementary Table 2). Plasmids are listed in Supplementary Table 3 while oligonucleotides used in plasmid construction are listed in Supplementary Table 4.

Dom34 and upstream flanking sequence were amplified from genomic DNA using primers OBS2597 and OBS2598 and cloned between the XhoI and XbaI sites of pRS415, giving pBS3217. Hbs1 with its flanking sequences was amplified from genomic DNA using primers OBS3474 and OBS3475 and cloned between the SmaI and HindIII sites of pRS415, generating pBS3611. C-terminal tags (3HA for Dom34 and ProtA for Hbs1) were introduced by fusion PCR. (For primers and templates used see Supplementary Table 5.) The Dom34-3HA product digested by HindIII and NheI was cloned into pBS3217, generating pBS3685. The Hbs1-ProtA product digested by NdeI and HindIII was cloned into pBS3611, generating pBS3614.

Dom34 and Hbs1 point mutations were introduced in pBS3685 or pBS3614 respectively by QuickChange mutagenesis, except for the KKKR mutant, which was produced by fusion PCR, digested by HindIII and XhoI and cloned into pBS3685 (see Supplementary Table 5 for primers and templates).

Dom34 Δ domain1 (amino acids 1-136 deleted) and Dom34 Δ domain2 (amino acids 141-275 replaced by (Gly)₄) domain deletion mutants were produced by fusion PCR (see Supplementary Table 5). The resulting fragments were digested by XhoI and NheI and cloned into pBS3217. Dom34 Δ domain3 (amino acids 276-386 deleted) was produced by PCR with OBS3396 and OBS3397 using pBS3217 as template. The resulting fragment digested by BglII/NheI was cloned into pBS3217. Dom34 domain

deletion mutants were amplified with the introduction of a C-terminal strep-tag using OBS3440 and OBS3171 (Dom34 Δ domain1), OBS3170 and OBS3171 (Dom34 Δ domain2) or OBS3170 and OBS3443 (Dom34 Δ domain3), digested with NdeI and KpnI and cloned into a pACYC-LIC+ vector. All constructs were verified by sequencing.

RNA analysis

Yeast cultures were grown in CSM-Leu-Ura (NGD assay) or CSM-Leu-Trp (18S NRD assay) containing 2% (w/v) galactose at 30 °C until OD₆₀₀ 0.6-1.2. Total RNA was obtained by hot phenol extraction, 10 μ g RNA was separated on 1.5% (w/v) agarose- 6.3% (w/v) formaldehyde gel (18S NRD) or 15 μ g on 1,25% agarose-6, 7% formaldehyde gel with bridges of Whatman paper separating gel from running buffer (NGD) and transferred to a HybondTM-XL membrane (GE Healthcare) as described earlier⁴⁰. Probe FL125 was 5' labeled with T4 polynucleotide kinase (Fermentas) and γ -32P ATP. For detection of endogenous scR1 and the PGK1-SL reporter probes were made by a random priming reaction on a PCR product obtained with primers OBS1884 / OBS1885 and OBS4139 / OBS4164 respectively using the Neblot[®] kit (New England Biolabs) and α -32P dCTP. Prehybridization and hybridization of the membranes with the labeled probes was performed in Church buffer at 42 °C and 40 °C respectively (NRD), at 55 °C (scR1) or at 65 °C (PGK1-SL). Signals were visualized with a Typhoon 8600 Variable Mode Imager (Molecular Dynamics) and quantified using ImageQuant 5.2 software.

References.

1. Doma, M.K. & Parker, R. RNA quality control in eukaryotes. *Cell* **131**, 660-8 (2007).
2. Isken, O. & Maquat, L.E. Quality control of eukaryotic mRNA: safeguarding cells from abnormal mRNA function. *Genes Dev* **21**, 1833-56 (2007).
3. Amrani, N., Sachs, M.S. & Jacobson, A. Early nonsense: mRNA decay solves a translational problem. *Nat Rev Mol Cell Biol* **7**, 415-25 (2006).
4. Frischmeyer, P.A. et al. An mRNA surveillance mechanism that eliminates transcripts lacking termination codons. *Science* **295**, 2258-61 (2002).
5. van Hoof, A., Frischmeyer, P.A., Dietz, H.C. & Parker, R. Exosome-mediated recognition and degradation of mRNAs lacking a termination codon. *Science* **295**, 2262-4 (2002).
6. Bengtson, M.H. & Joazeiro, C.A. Role of a ribosome-associated E3 ubiquitin ligase in protein quality control. *Nature* **467**, 470-3 (2010).
7. Doma, M.K. & Parker, R. Endonucleolytic cleavage of eukaryotic mRNAs with stalls in translation elongation. *Nature* **440**, 561-4 (2006).
8. Gandhi, R., Manzoor, M. & Hudak, K.A. Depurination of Brome mosaic virus RNA3 in vivo results in translation-dependent accelerated degradation of the viral RNA. *J Biol Chem* **283**, 32218-28 (2008).
9. LaRiviere, F.J., Cole, S.E., Ferullo, D.J. & Moore, M.J. A late-acting quality control process for mature eukaryotic rRNAs. *Mol Cell* **24**, 619-26 (2006).
10. Cole, S.E., LaRiviere, F.J., Merrikh, C.N. & Moore, M.J. A convergence of rRNA and mRNA quality control pathways revealed by mechanistic analysis of nonfunctional rRNA decay. *Mol Cell* **34**, 440-50 (2009).
11. Soudet, J., Gelugne, J.P., Belhabich-Baumas, K., Caizergues-Ferrer, M. & Mouglin, A. Immature small ribosomal subunits can engage in translation initiation in *Saccharomyces cerevisiae*. *Embo J* **29**, 80-92 (2010).
12. Carr-Schmid, A., Pfund, C., Craig, E.A. & Kinzy, T.G. Novel G-protein complex whose requirement is linked to the translational status of the cell. *Mol Cell Biol* **22**, 2564-74 (2002).
13. Adham, I.M. et al. Disruption of the pelota gene causes early embryonic lethality and defects in cell cycle progression. *Mol Cell Biol* **23**, 1470-6 (2003).
14. Davis, L. & Engebrecht, J. Yeast dom34 mutants are defective in multiple developmental pathways and exhibit decreased levels of polyribosomes. *Genetics* **149**, 45-56 (1998).
15. Eberhart, C.G. & Wasserman, S.A. The pelota locus encodes a protein required for meiotic cell division: an analysis of G2/M arrest in *Drosophila* spermatogenesis. *Development* **121**, 3477-86 (1995).
16. Xi, R., Doan, C., Liu, D. & Xie, T. Pelota controls self-renewal of germline stem cells by repressing a Bam-independent differentiation pathway. *Development* **132**, 5365-74 (2005).
17. Graille, M., Chaillet, M. & van Tilbeurgh, H. Structure of yeast Dom34: a protein related to translation termination factor ERF1 and involved in No-Go decay. *J Biol Chem* **283**, 7145-54 (2008).
18. Lee, H.H. et al. Structural and functional insights into Dom34, a key component of No-Go mRNA decay. *Mol Cell* **27**, 938-50 (2007).
19. Passos, D.O. et al. Analysis of Dom34 and Its Function in No-Go Decay. *Mol Biol Cell* (2009).
20. Atkinson, G.C., Baldauf, S.L. & Haurlyliuk, V. Evolution of nonstop, no-go and nonsense-mediated mRNA decay and their termination factor-derived components. *BMC Evol Biol* **8**, 290 (2008).
21. Wallrapp, C. et al. The product of the mammalian orthologue of the *Saccharomyces cerevisiae* HBS1 gene is phylogenetically related to eukaryotic release factor 3 (eRF3) but does not carry eRF3-like activity. *FEBS Lett* **440**, 387-92 (1998).
22. Nelson, R.J., Ziegelhoffer, T., Nicolet, C., Werner-Washburne, M. & Craig, E.A. The translation machinery and 70 kd heat shock protein cooperate in protein synthesis. *Cell* **71**, 97-105 (1992).
23. Inagaki, Y., Blouin, C., Susko, E. & Roger, A.J. Assessing functional divergence in EF-1alpha

- and its paralogs in eukaryotes and archaeobacteria. *Nucleic Acids Res* **31**, 4227-37 (2003).
24. Pisareva, V.P., Pisarev, A.V., Hellen, C.U., Rodnina, M.V. & Pestova, T.V. Kinetic analysis of interaction of eukaryotic release factor 3 with guanine nucleotides. *J Biol Chem* **281**, 40224-35 (2006).
 25. Kong, C. et al. Crystal structure and functional analysis of the eukaryotic class II release factor eRF3 from *S. pombe*. *Mol Cell* **14**, 233-45 (2004).
 26. Vetter, I.R. & Wittinghofer, A. The guanine nucleotide-binding switch in three dimensions. *Science* **294**, 1299-304 (2001).
 27. Nissen, P. et al. Crystal structure of the ternary complex of Phe-tRNA^{Phe}, EF-Tu, and a GTP analog. *Science* **270**, 1464-72 (1995).
 28. Leibundgut, M., Frick, C., Thanbichler, M., Bock, A. & Ban, N. Selenocysteine tRNA-specific elongation factor SelB is a structural chimaera of elongation and initiation factors. *Embo J* **24**, 11-22 (2005).
 29. Song, H., Parsons, M.R., Rowsell, S., Leonard, G. & Phillips, S.E. Crystal structure of intact elongation factor EF-Tu from *Escherichia coli* in GDP conformation at 2.05 Å resolution. *J Mol Biol* **285**, 1245-56 (1999).
 30. Cheng, Z. et al. Structural insights into eRF3 and stop codon recognition by eRF1. *Genes Dev* **23**, 1106-18 (2009).
 31. Petoukhov, M.V. & Svergun, D.I. Global rigid body modelling of macromolecular complexes against small-angle scattering data. *Biophys J* (2005).
 32. Kononenko, A.V. et al. Role of the individual domains of translation termination factor eRF1 in GTP binding to eRF3. *Proteins* **70**, 388-93 (2008).
 33. Alkalaeva, E.Z., Pisarev, A.V., Frolova, L.Y., Kisselev, L.L. & Pestova, T.V. In vitro reconstitution of eukaryotic translation reveals cooperativity between release factors eRF1 and eRF3. *Cell* **125**, 1125-36 (2006).
 34. Haurlyuk, V., Zavialov, A., Kisselev, L. & Ehrenberg, M. Class-1 release factor eRF1 promotes GTP binding by class-2 release factor eRF3. *Biochimie* **88**, 747-57 (2006).
 35. Pisarev, A.V. et al. The role of ABCE1 in eukaryotic posttermination ribosomal recycling. *Mol Cell* **37**, 196-210 (2010).
 36. Salas-Marco, J. & Bedwell, D.M. GTP hydrolysis by eRF3 facilitates stop codon decoding during eukaryotic translation termination. *Mol Cell Biol* **24**, 7769-78 (2004).
 37. Seraphin, B. Sm and Sm-like proteins belong to a large family: identification of proteins of the U6 as well as the U1, U2, U4 and U5 snRNPs. *Embo J* **14**, 2089-98 (1995).
 38. Wilusz, C.J. & Wilusz, J. Eukaryotic Lsm proteins: lessons from bacteria. *Nat Struct Mol Biol* **12**, 1031-6 (2005).
 39. Song, H. et al. The crystal structure of human eukaryotic release factor eRF1--mechanism of stop codon recognition and peptidyl-tRNA hydrolysis. *Cell* **100**, 311-21 (2000).
 40. Prouteau, M., Daugeron, M.C. & Seraphin, B. Regulation of ARE transcript 3' end processing by the yeast Cth2 mRNA decay factor. *Embo J* **27**, 2966-76 (2008).

Figure 1.

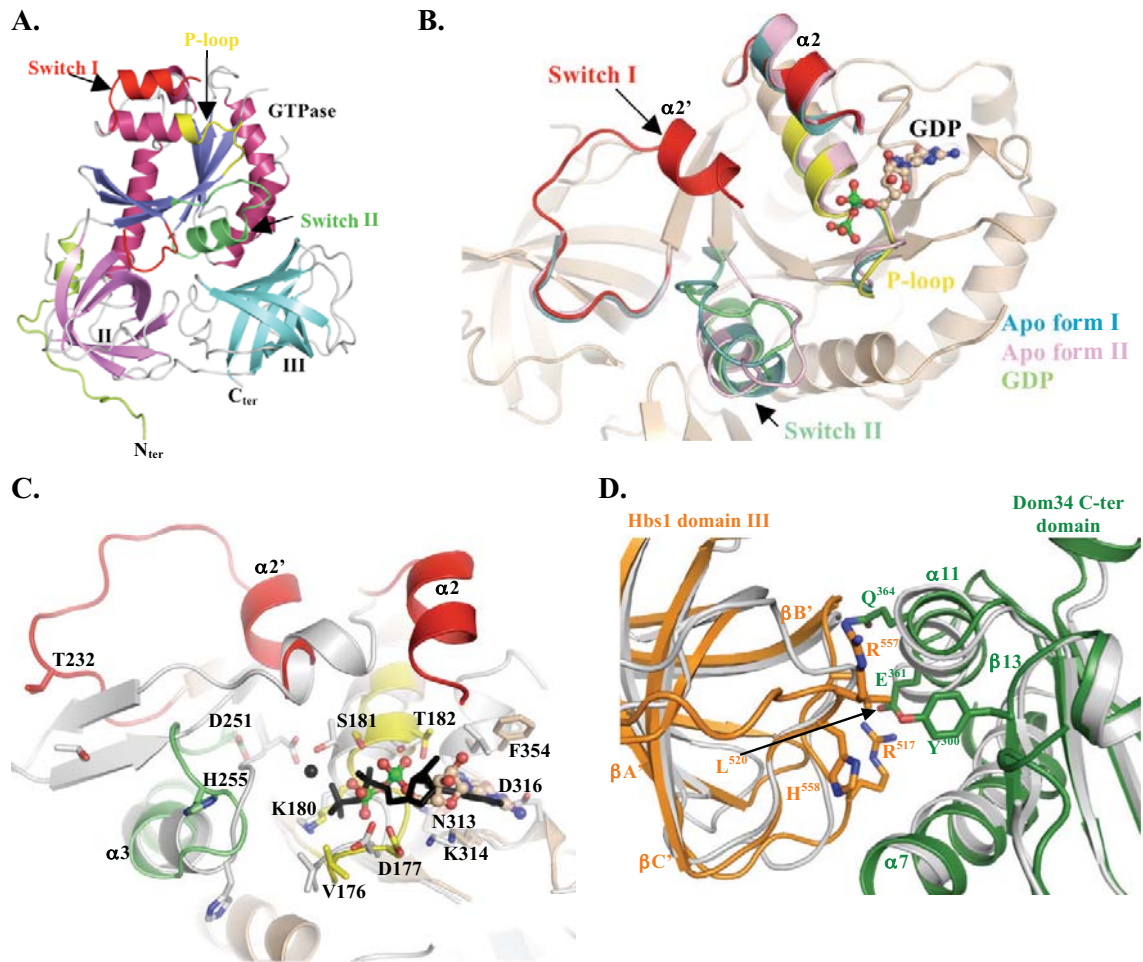


Figure 2.

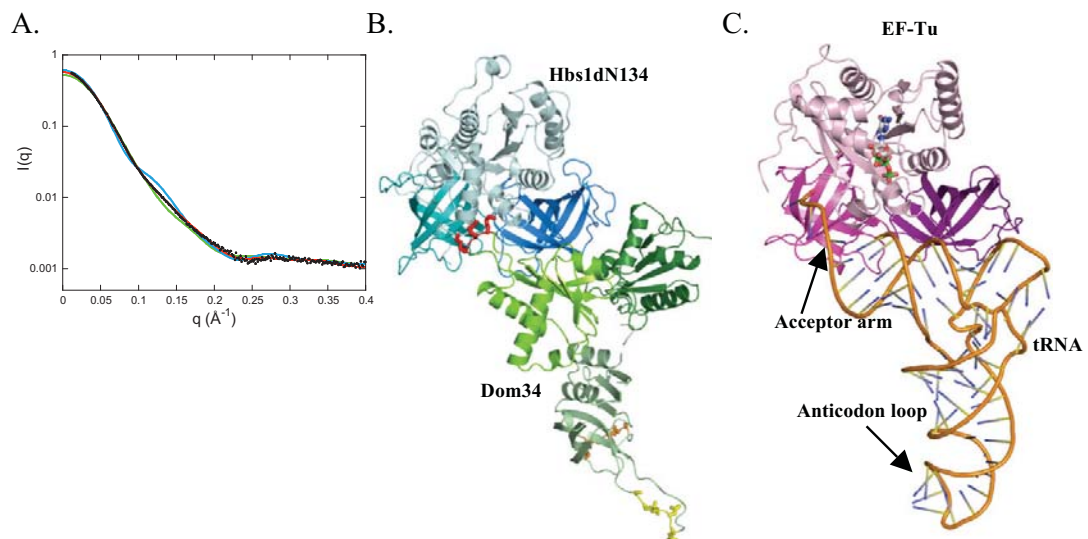
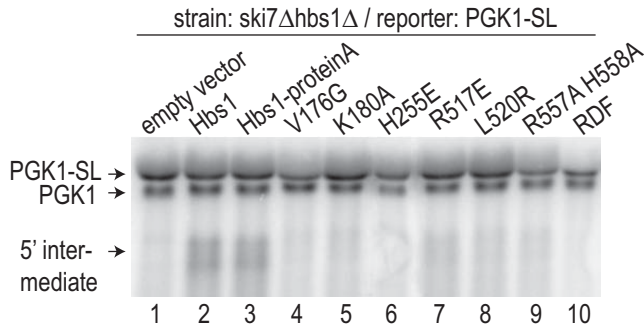
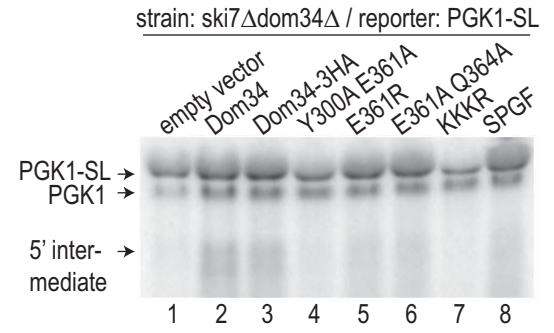


Figure 3.

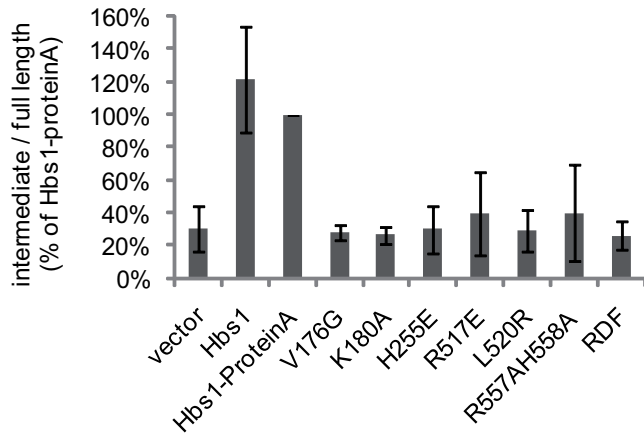
a



b



c



d

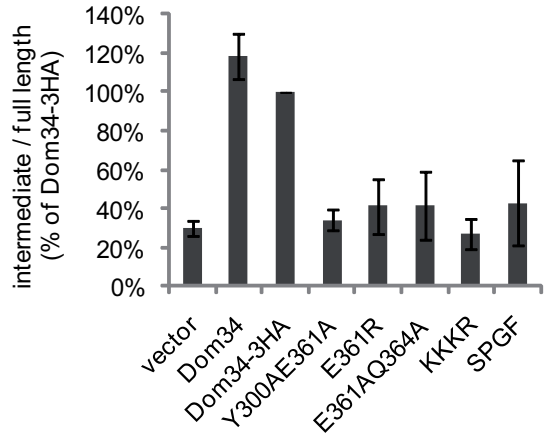
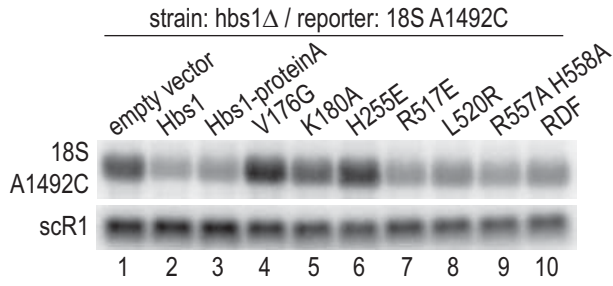
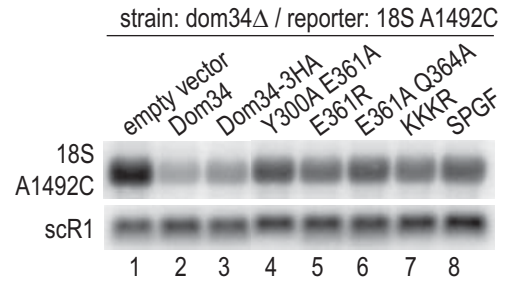


Figure 4.

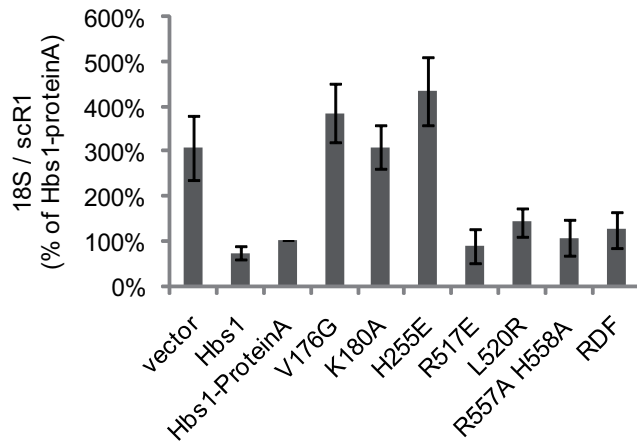
a



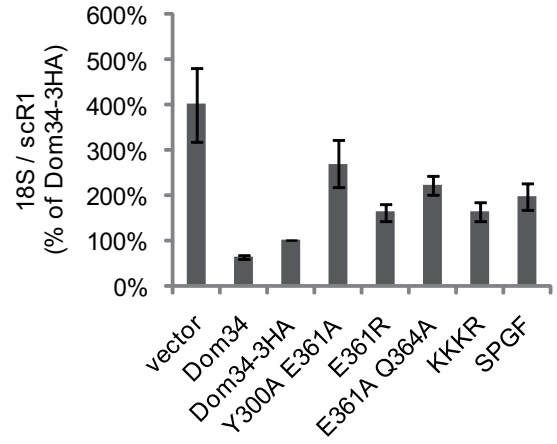
b



c



d



e

